energy&fuels

Article

Cite This: *Energy Fuels* 2019, 33, 12801−12813

pubs.acs.org/EF

Numerical Investigation on the Improvement of Carbon Conversion in a Dual Circulating Fluidized Bed Reactor for Chemical Looping Combustion of Coal

Xi Chen, Jinchen Ma, Xin Tian, Zuwei Xu, and Haibo Zhao*

State Key Laboratory of Coal Combustion, School of Energy and Power Engineering, Huazhong University of Science and Technology, Wuhan, Hubei 430074, People's Republic of China

Supporting Information

ABSTRACT: A dual circulating fluidized bed reactor for chemical looping combustion of coal has the advantage of flexible regulation on oxygen carrier circulation, but there is always part of unconverted coal char escaping from the fuel reactor (FR), reducing the carbon capture efficiency of the whole unit. In this work, a numerical investigation is conducted using the computational particle fluid dynamics (CPFD) method to examine how to improve the carbon conversion in a 50 kW_{th} coal-fueled dual circulating fluidized bed reactor for chemical looping combustion. The improvement strategies generally fall into two categories. The first category is based on the ideas of extending the residence time of char and strengthening the mixing between the char and oxygen carrier (OC), including enhancing the FR height, increasing the number of coal feeding points, and leading combustible gas generated in the gasification carbon stripper (GCS) to the FR. The second category is to physically separate char particles from the binary material stream in a carbon striper (CS) based on the difference of terminal velocity between the char and OC particles and then recycle the stripped char to the FR again. With respect to the 50 kW_{th} reactor, in which a two-chamber GCS is coupled within the loop seal, the full-scale CPFD simulation reveals that, when the GCS is off, the carbon capture efficiency (solely contributed by the FR) is quite low (42.3%), even if some optimizations are adopted for the FR (two oppositely collocated coal feeding points, 56.4%; doubling the FR height, 58.7%). On the other side, when the GCS is on, the carbon capture efficiency reaches over 90% significantly. To further improve the carbon conversion in the reactor, a new non-mechanical valve integrated with a four-chamber CS/GCS is designed numerically in this paper, where three-dimensional CFPD simulation is conducted to optimize the key parameters, such as freeboard height, baffle height, flow rate of OC, and superficial velocity. The integrated and compact device can function as the loop seal and carbon stripper simultaneously, and it can be operated as not only the CS mode (char is physically separated from OC) but also the GCS mode (char is gasified, and then combustible products are recycled back to the FR; i.e., char is chemically separated from OC) by regulating the operational velocity and fluidization agent. The carbon capture efficiencies of GCS and CS modes are 97.8 and 98.9%, respectively. The CS mode is more economical in terms of the operational cost, because a large amount of steam is not required herein. Finally, by means of parallel comparisons on these strategies mentioned above in performance and cost, the optimal strategy to improve carbon conversion in the reactor is proposed successfully.

1. INTRODUCTION

Chemical looping combustion (CLC) technologies are regarded as the promising means for low-carbon utilization of carbon-containing energy as a result of its inherent separation of CO_2, in which *in situ* gasification chemical looping combustion (*i*G-CLC) allows for the combustion of solid fuels, such as coal, in a direct and economical way. Typically, the *i*G-CLC process employs a dual circulating fluidized bed (DCFB) reactor, which can regulate the material circulation rate in a more flexible way. In the process, metal oxide particles are used as the oxygen carrier (OC) to transfer the lattice oxygen from one reactor to the other, which are called the air reactor (AR) and the fuel reactor (FR), respectively. The FR is fluidized by a gasification agent, such as CO_2 or H_2O, for the involved intermediate gasification step of remaining char after volatile release, and the OC is reduced by these combustible gases. The AR is fluidized by air, and the OC is oxidized/regenerated. Several different prototypes of the DCFB reactor have been successfully proposed and demonstrated in the past 10 years.[1−4] However, there are also some key targets to be solved in relation to the FR performance, mainly in the fuel conversion process, namely, carbon conversion, such as gas conversion and char slip.[5,6] In terms of gas conversion, it can be classified as two types. First, the volatiles are released as a plume, and the reactions between the OC and volatiles occur in the limited volume of the plume, which is affected by superficial gas velocity. Second, the char gasification process happens in the whole FR, and it is influenced by the mixture of OC and char particles. Usually, there is an amount of unconverted gases escaping from the FR inevitably with the bypassing of bubbles, reducing the combustion efficiency of the whole unit. Meanwhile, for the issue of char slip in the reactor, the rate of char gasification is much slower than the rate of OC reduction. Namely, char gasification is the limitation step, and char particles require a relatively long residence time for complete conversion. The

Received: September 2, 2019
Revised: November 6, 2019
Published: November 21, 2019

DOI: 10.1021/acs.energyfuels.9b02963
Energy Fuels 2019, 33, 12801−12813

Table 1. Summary of the Constructed CS in the Literature

authors	CS type	CS size	fluidization regime	unit size	location
Berguerand et al.[21]	two-chamber CS coupled with FR	cross section, 0.037 × 0.044 m	bubbling regime	10 kW_{th}	Chalmers University of Technology
Markström et al.[22]	four-chamber CS	cross section, 0.3 × 0.3 m	bubbling regime	100 kW_{th}	Chalmers University of Technology
Abad et al.[25]	cylindrical CS with a transition zone	diameter, 0.15 m; height, 0.71 m	bubbling regime	20 kW_{th}/50 kW_{th}	CSIC
Sun et al.[27]	four-chamber CS with a transition zone	cross section, 0.3 × 0.3 m; height, 0.3 m	bubbling regime	70 kW_{th}	Tsinghua University
Sun et al.[5]	riser-based CS	diameter, 0.03 m; height, 4.03 m	fast fluidization regime	70 kW_{th}	Tsinghua University
Cheng et al.[28]	annular CS	diameter of the center riser, 0.02 m; diameter of the annular zone, 0.07 m	fast fluidization regime	30 kW_{th}	Tsinghua University
Abdulally et al.[29]	three-chamber CS		bubbling regime	1 MW_{th}	Alstom Power, Inc.
Ströhle et al.[12]	rectangular CS		bubbling regime	1 MW_{th}	Darmstadt University of Technology
Ma et al.[30]	two-chamber CS coupled within a loop seal	cross section, 0.19 × 0.4 m; height, 0.8 m	bubbling regime	50 kW_{th}	Huazhong University of Science and Technology

carbon capture efficiency will reduce if char particles are entrained by the OC stream to the AR, where the char will be burnt out by O_2. The products (CO_2, NO_x, SO_x, etc.) of char combustion will mix with the AR flue gases, and it is not economical and environmentally friendly for further processing. In brief, there are plenty of works for the improvement of carbon conversion in the *i*G-CLC technology.

Several kinds of strategies have been proposed to improve combustible gas conversion,[5−7] focusing on intensifying and prolonging the conversion of gaseous fuel, including optimizing the operational parameters,[8−11] oxygen polishing,[12] employing two-stage FR,[13−16] intensifying the gas−solid contact by internals or optimizing the structure of the FR,[15,17−19] recycling the combustible gases separated from the process of CO_2 liquefaction to the FR again, using another kind of OC with higher reactivity,[20] etc. Gayán et al.[7] evaluated several technological solutions for improving the combustion efficiency of the *i*G-CLC process through macroscopic fuel reactor modeling, involving most of the measures listed above. Simulations showed that the use of a secondary fuel reactor was superior to others on reducing the unburnt compounds in the flue gas stream. Furthermore, a new configuration employing the carbon stripper (CS) as a secondary FR and leading the exhaust gases from the primary FR to the CS was proposed. The carbon capture efficiency and oxygen demand were predicted to be 98.8 and 0.9%, respectively.

For the issue of char slip, there are also two typical strategies to prevent unconsumed char from escaping to the AR along with material stream. The first strategy is to extend the reaction route to guarantee sufficient residence time for the char gasification reaction, which can be arranged in not only the single FR, namely, changing the FR structure to increase the char residence time, but also the supplementary devices, such as gasification carbon stripper (GCS), secondary FR, etc. Another strategy is to separate char particles from material stream in a physical way according to the difference of terminal velocity in the binary mixture system and then recycle these char particles to the FR again. This process occurs in the CS, which can be fluidized with or without a gasification agent. If the gasification agent (CO_2 and/or H_2O) is introduced into the CS, char will be gasified and then combustible products can be recycled back to FR, which means char is chemically separated from the main stream. In this case, if the operational velocity is lower than the terminal velocity of char particles, the physical separation will not happen in the device. To distinguish it from conventional CS (where char is physically separated from OC), this kind of CS (with a gasification agent) is called as GCS in this paper. Obviously, the main distinction between these two strategies to prevent char slip is that the first strategy is an open loop of char circulation with the consumption of char along the unidirectional route, whereas the CS strategy constructs a closed loop between the FR and CS. Until now, various prototypes have been proposed to prevent the char slip in the *i*G-CLC unit. Basically, those pilot plants prefer to employ the CS strategy as the mainly optimization to prevent char slip than only focusing on extending the residence time of char in the FR, because the residence time is difficult to be predicted and controlled. Factually, the strategy of extending the reaction route is always incorporated initially in the design process, and there are few studies focusing on this problem. A conceptual 1000 MW_{th} CLC boiler designed by Lyngfelt and Leckner[6] did not consider a specified CS but a enough long transport distance between the fuel feed location and the exit of bed material at the bottom of the FR. Fuel particles move in the opposite direction of OC; thus, the transport distance will provide enough time both for reaction and separation of char particles. Finally, the char fines are stripped, moving upward with the fluidization gas.

In terms of the CS strategy, several kinds of prototypes from different institutes are summarized in Table 1. At Chalmers University of Technology, Lyngfelt and his colleagues[21,22] reported two kinds of carbon separation configurations. The primary configuration is a two-chamber CS integrated within the FR in a 10 kW_{th} CLC unit, and the second configuration is a serial four-chamber CS separated by weirs, which is able to prevent the char floating on the surface of the dense bed from bypassing the chambers, prolonging the residence time of char in the CS. It can be fluidized with/without a gasification agent, and the contribution of the gasification in CS was also experimentally evaluated as much as 3%.[22] This kind of serial four-chamber CS was later widely accepted in other pilot

DOI: 10.1021/acs.energyfuels.9b02963
Energy Fuels 2019, 33, 12801−12813

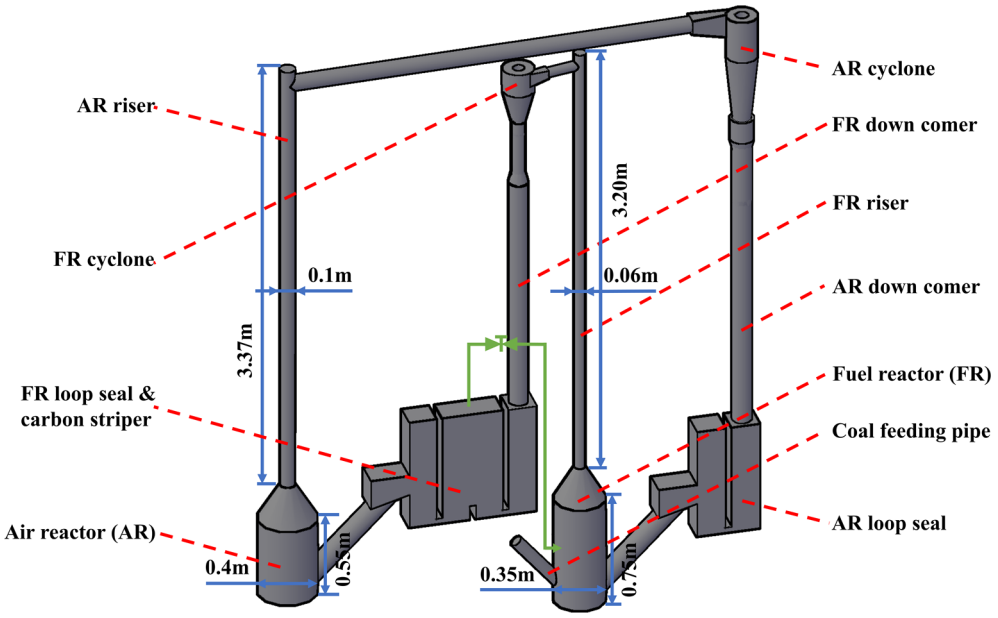

Figure 1. Structure of the 50 kW_{th} CLC reactor.

plants because of the balance between complexity and performance. In CSIC, Mendiara et al.[23] concluded that the CS reduces sulfur and nitrogen emissions in the AR and suggested the CS as a crucial component in the CLC reactor of solid fuel. Abad et al.[24] constructed a macroscopic model of the FR with a CS and evaluated the effect of a carbon separation system on the operational performance. Then, they designed and constructed a CLC unit,[25] which can be operated in both *i*G-CLC (20 kW_{th}) and chemical looping with oxygen uncoupling (CLOU) (50 kW_{th}) modes with a CS working in the bubbling fluidized regime. The residence time of solids in the CS was estimated to be 100 s, and the carbon capture efficiency was measured as 88%. Later, a further study on the conceptual design for the scale-up of industrial installation, meanwhile preventing char slip, was also proposed. Abad et al.[26] put forward a 100 MW_{th} CLC unit for solid fuel combustion, in which a CS was considered as a bubbling fluidized bed with a cross section of 30 m^2 and bed inventory of 46 000 kg. The gas velocity was assumed to be 0.65 m/s for a quite high separation efficiency of 98%. Moreover, Sun et al.[27] in Tsinghua University presented a four-chamber CS with an additional transition zone at the top of it in the cold flow model of a 70 kW CLC reactor. The separation characteristics of the CS were studied in a long-term operation, changing operational factors and the CS inner structure. The separation efficiency of the CS was up to 60%, and 160% additional residence time of the fuel particles was achieved. They also designed a riser-based CS[5] operated in a high-velocity regime, which is quite different from other prototypes, and a high separation efficiency was reported. In this work, an analysis on the advantages of different strategies to prevent char slip was conducted. Following that, a similar annular CS was investigated by Cheng et al.[28] The char particles are separated by the riser in the center; meanwhile, the OC particles drop down to the outer annular fluidized bed. Apart from these studies, there are also some works involving preventing char slip by the CS strategy, such as the unit constructed by Ströhle et al.[12] and Abdulally et al.[29] To summarize, on the basis of the review of these CS prototypes, it can be found that the available CS was typically designed as an individual device and was arranged between two loop seals in series. This type of arrangement is not compact and introduces more complexity for the regulation of solid circulation; therefore, it may be more difficult to build a steady pressure balance. On the basis of these considerations, in our 50 kW_{th} reactor,[30] a two-chamber GCS was coupled between the supply chamber and recycle chamber of a loop seal (LS) to simplify the structure and circulation regulation. In the design, the integrated CS + LS was fluidized by 50 vol % H_2O + 50 vol % N_2; therefore, it can work as a GCS to recycle these gasification products back to the FR.

It is generally accepted that the performance of the CLC process in DCFB should be promoted to achieve better targets, such as carbon capture efficiency and CO_2 yield, and there are already various kinds of strategies proposed for the objective. Before the adoption of a specified strategy on a real device, detailed investigations are necessary. However, few works focused on the parallel comparison of different strategies or various optimizations of a specified strategy as a result of many limitations of experimental research. The computational fluid dynamics (CFD) method, which has more considerable advantages in the analysis of details than the experimental measurement, is quite suitable for these kinds of issues. Among all of the branches of CFD approaches, the computational particle fluid dynamics (CPFD) method is an effective and competitive tool to simulate the gas−solid flow in the model with massive particles and multiple fluidization regimes. The CPFD method was developed on the basis of the Eulerian−Lagrangian method by Andrews and O'Rourke[31] and Snider.[32] In this methodology, the fluid equations are solved in the Eulerian approach on the mesh and particles, which are considered as the computational parcel containing a group of particles, are solved in the Lagrangian manner with the implementation of the multiphase particle-in-cell (MP-PIC) method. Significant works were conducted in the CLC community using CFD[33,34] and CPFD[19,35] methods, involving not only the single FR but also the whole unit in cold and hot models with different combinations of the OCs and fuels.

DOI: 10.1021/acs.energyfuels.9b02963
Energy Fuels 2019, 33, 12801−12813

Generally, they mainly focused on the development and validation of accurate gas−solid reaction kinetics,[36,37] reasonable heterogeneous models on gas−solid interaction,[38,39] and optimizations of operation based on the hydrodynamics in the reactor.[40]

Taking the panoramic view of the simulations about *i*G-CLC, few works pay attention to the carbon conversion in the unit and how to promote it. Therefore, in this work, the CPFD method is employed to study the carbon conversion process, especially char conversion, and how to promote it in the 50 kW_{th} DCFB reactor for *i*G-CLC of coal. Initially, the 50 kW_{th} reactor with a two-chamber GCS coupled between the supply chamber and recycle chamber of a loop seal is numerically evaluated in terms of carbon conversion. It can be found that the carbon capture efficiency of a single FR is quite low because of char slip, even if some optimizations are adopted for the FR, like increasing coal feeding points and FR height. However, when the GCS works, the carbon capture efficiency increases significantly. However, there is still room for the improvement of the original GCS, such as improving the char conversion and reducing the operational cost. Therefore, a new device is designed as a non-mechanical valve with four-chamber CS/GCS by the numerical method. It can be operated as not only the CS mode but also the GCS mode by regulating the operational velocity and fluidization agent. For these strategies mentioned above to optimize carbon conversion, investigations are conducted to compare the carbon conversion and operational cost of different strategies in details. Finally, the optimal strategy is selected to meet the balance between performance and cost.

2. SIMULATION MODEL

A schematic view of the 50 kW_{th} DCFB reactor for *i*G-CLC is shown in Figure 1. It is constituted by two main parts, namely, the AR and FR. There are other components with the functions of connection, separation, and transportation, including risers, down comers, cyclones, CS, and loop seals. At the top of the AR and FR, there is a transition zone connecting with the riser to increase the local gas velocity and maintain a relatively high solid circulation rate. The CS is integrated with the LS of FR to compact the system structure, and it is arranged between the supply chamber and recycle chamber of the LS, which can reduce the pressure fluctuation in the CS and keep it operating steadily. Besides, the supply chambers + down comers are designed with a large size to accommodate enough bed materials to endow the unit with the ability of self-adjustment. On the basis of the observation in simulation and experiment, the bed inventory in the supply chamber and down comer can be 60−90 kg.[19] The supply chamber is operated as a moving bed with the superficial velocity closing to the minimum fluidization velocity, and if the fluidization agent of it is changed to CO_2/H_2O, the supply chamber + down comer will become an extra place for the *i*G-CLC process, i.e., extending the reaction route as well as the residence time of char particles. The dimension of the simulation model is the same as the actual reactor, and the main sizes of the reactor are listed in Figure 1.

The governing equations of the CPFD model on hydrodynamics and the reactive kinetics involved in the simulation can be seen in our previous publication[19] and also summarized in the Supporting Information. The involved reactions include coal pyrolysis, char gasification with CO_2/H_2O, heterogeneous reactions between OC and fuel gases, OC oxidation, residual char combustion, and water−gas shift reaction. Natural hematite is used as the OC; Shenhua bituminous coal is used as fuel; and the properties of the OC and coal are shown in Table 2. Steam is adopted as the gasification agent with which the char gasification reaction is faster than that with CO_2. Initially, OC is stacked at the bottom of the reactor with the closely packed solid volume fraction of 0.625, and the bed inventories in the AR, FR, AR supply chamber + down comer, and FR supply chamber + down comer are 88, 143.5, 84.5, and 73.8 kg, respectively. The initial bed inventory adopted in simulations refers to the OC redistribution undergoing a dynamic balance, which can reduce the simulation time to reach a steady state. The operational temperature is 1273 K, and the heat needed in this unit is supplied by the electric heater. The coal is fed from the coal feeding pipe, and the feeding rate is 7.3 kg/h. The AR is fluidized by air with the superficial velocity of 0.585 m/s (0.5 U_t, where U_t is the terminal velocity of OC particles), and the FR is fluidized by 50 vol % N_2 + 50 vol % H_2O with the velocity of 0.3 m/s (15 U_{mf}, where U_{mf} is the minimum fluidization velocity of OC particles). The LS of AR is fluidized by N_2, and the superficial velocity of the recycle chamber and supply chamber is 0.144 and 0.072 m/s, respectively. However, the fluidization agent and operational velocity of FR LS and CS/GCS are changed for different functions, and these working conditions are specified in Table 3 in the following part. The pressure at the outlet of the cyclone is 101 325 Pa. Before simulation, the independence of mesh, particle resolution, and time step are evaluated on the exhaust concentration and FR pressure file, and finally, the cell number of 476 000 with 2 139 908 particles is adopted. The time step is 0.000 01 s under GPU parallel computing. Then, to validate the model, a series of comparisons are conducted with the data obtained in the simulation and experiment. The results show that the model can predict the details in the reactor on hydrodynamics and chemical reactions in a relatively accurate way, and the details of model validation can be seen in the Supporting Information.

Table 2. Composition and Properties of OC and Coal Used in the Experiment and Simulation

Composition Analysis (wt %, ad) of OC			
Fe_2O_3	SiO_2	CaO	others
90.09	3.41	5.33	1.17
OC Properties			
radius range	150−350 μm	density	3650 kg/m^3
Proximate Analysis (wt %, ad) of Coal			
fix carbon	48.46	volatile matter	15.54
moisture	1.66	ash	34.34
Ultimate Analysis (wt %, ad) of Coal			
C	55.26	H	2.12
O	5.39	N	0.79
S	0.44		
Coal Properties			
radius range	100−300 μm	density	1346 kg/m^3

3. STRATEGIES TO IMPROVE CARBON CONVERSION

3.1. General Introduction. As mentioned above, the purpose of this paper is to investigate the carbon conversion, especially char conversion, in the 50 kW_{th} DCFB reactor for *i*G-CLC. To prevent the char slip, several feasible strategies are proposed and compared employing the CPFD method, as seen

DOI: 10.1021/acs.energyfuels.9b02963
Energy Fuels 2019, 33, 12801−12813

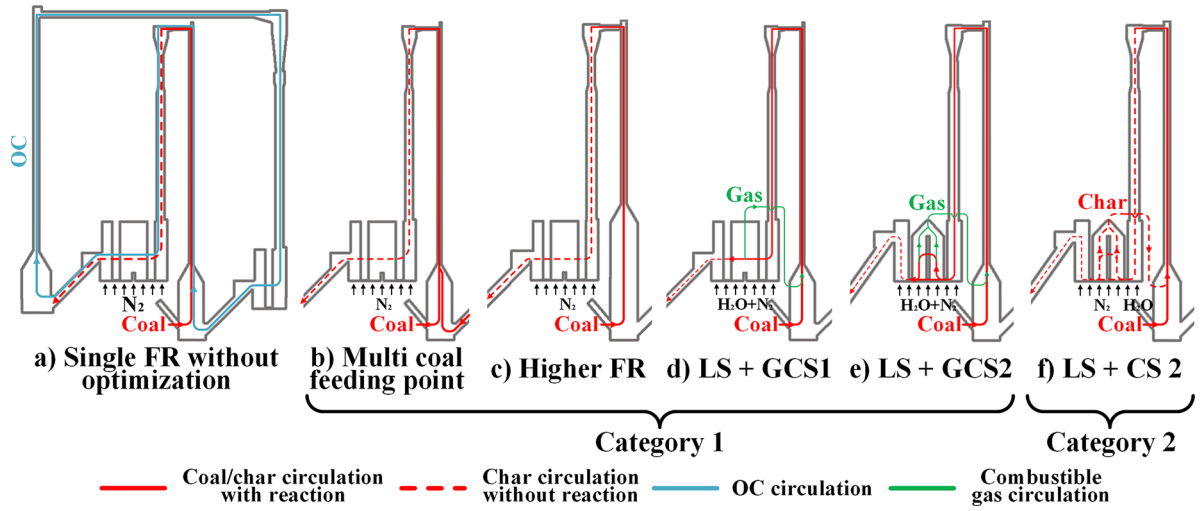

Figure 2. Strategies to improve the carbon conversion in a CLC reactor.

in Figure 2 and Table 3, where Figure 2 shows the sketch of different strategies and Table 3 shows the parallel comparison of them on principles and operational conditions. As schematically shown in Figure 2a, in the 50 kW_{th} unit without optimization, OC flows along the loop of material circulation, which can transport lattice oxygen and reaction heat from one reactor to another (the reaction heat can be neglected in this work compared to the heat from the electrical heater). The char generated in the coal pyrolysis, which entirely happens in the FR, is entrained by the OC stream from the FR to the AR. The gasification happens in the FR and FR riser, whereas the reaction in the FR riser can be neglected because of the high velocity and, consequently, short residence time of char particles. The oxidization of fuel gases almost happens in the FR as well. Hence, the extent of carbon conversion under this circumstance depends upon the residence time of char particles and fuel gases as well as the gas−solid contact in the FR. On the basis of the simulation results, the residence time of char in the FR of Figure 2a is relatively short and the gas−solid contact should also be optimized. The carbon capture efficiency of a single FR without optimization (meanwhile, the GCS is off) is only 42.3%, but the CO_2 yield is 94.1%, Therefore, how to prevent char slip, i.e., how to promote carbon conversion, is prior to other issues.

In response to this issue, two methods were proposed to optimize the FR at first, as described in our previous publication.[19] The first method adopts the two oppositely collocated coal feeding points in Figure 2b. The volatile plume and char can disperse more widely and uniformly in the FR. It is equivalent to introduce another reaction route. For the fuel gases from char gasification, the new coal feeding mode intensifies the mixture and dispersity of char particles in the FR; therefore, the gas product conversion is also improved. The second method is to optimize the FR structure, especially FR height, in Figure 2c, and it is obvious that an increase of the FR height prolongs the residence time and reaction route of char and fuel gases. It has been revealed that the average residence time of char particles increases from 37 to 112 s with the increase of the FR height from 75 to 150 cm. In conclusion, the two optimizations only focus on the FR itself by extending the residence time and reaction route of fuel in it, and the char gasification in these two cases did not take place beside FR. Simulation results reveal that the carbon capture efficiencies of strategies b and c are 56.4 and 58.7%, respectively. The CO_2 yields are 95.8 and 97.2%, respectively. The gas and char conversion are all improved in comparison to strategy a, but there are almost half of carbon in char escaping to the AR; therefore, it is necessary to find other effective methods.

Apart from the strategies just focusing on the FR, there are other supplementary devices beyond the FR to prolong the residence time of char and improve char conversion, such as GCS and secondary FR. Therefore, a two-chamber GCS, which is coupled between the recycle chamber and supply chamber of the LS, was designed and constructed for the 50 kW_{th} reactor, like in strategy d (LS + GCS 1) in Figure 2. The GCS is not for physical separation of char particles; however, it is fluidized by N_2 + H_2O in a low superficial velocity for char gasification, and the gasification products are recycled back to the FR again. The supply chamber + down comer of the LS can also be fluidized by steam as a moving bed reactor because the residence time of char in it is relatively long. Therefore, the GCS 1 and LS can be considered as a secondary FR. Results from simulation have revealed that the carbon capture efficiency of the whole system significantly increases from 42.3 to 90.4%, but the improvement of the CO_2 yield is quite small (from 94.1 to 94.5%).

Despite the char slip being greatly relieved by the GCS 1, the *i*G-CLC performance, especially the carbon capture efficiency, should be further improved. A new six-chamber non-mechanical valve integrating the CS/GCS (four chambers in serial) and LS (two chambers) is designed in this work. With the change of the fluidization agent and operational velocity, the operational mode of this device can be switched between CS (as strategy f, LS + CS 2 in Figure 2) and GCS (as strategy e, LS + GCS 2 in Figure 2), as shown in Table 3. When it is operated as a CS, it can recycle the unconsumed char from the binary material stream to the FR; thus, a circulation between the FR and CS is established. In this case, with the recirculation of char particles, more and more char particles accumulate in the loop; therefore, the concentration of char increases gradually until the system reaches the dynamic balance between accumulation and consumption. The residence time of char will also increase with the circulation in the loop until char particles flow out of the FR cyclone or slip to the AR. When it is operated as a GCS in Figure 2e, the

DOI: 10.1021/acs.energyfuels.9b02963
Energy Fuels 2019, 33, 12801−12813

Table 3. Comparisons of Different Strategies to Promote Carbon Conversion

strategy	feature	principle	recycle chamber (fluidization agent/operational velocity)	CS/GCS (fluidization agent/operational velocity)	supply chamber (fluidization agent/operational velocity)
a	single FR	without optimization	N_2/0.144 m/s	N_2/0.054 m/s	N_2/0.072 m/s
b	multi-coal feeding point	extend reaction route/intensify gas−solid contact in the FR	N_2/0.144 m/s	N_2/0.054 m/s	N_2/0.072 m/s
c	higher FR	extend reaction route in the FR	N_2/0.144 m/s	N_2/0.054 m/s	N_2/0.072 m/s
d	LS + GCS 1 (four chambers)	extend reaction route beyond the FR	50 vol % N_2 + 50 vol % H_2O/0.144 m/s	50 vol % N_2 + 50 vol % H_2O/0.054 m/s	50 vol % N_2 + 50 vol % H_2O/0.072 m/s
e	LS + GCS 2 (six chambers)	extend reaction route beyond the FR	50 vol % N_2 + 50 vol % H_2O/0.144 m/s	50 vol % N_2 + 50 vol % H_2O/0.2 m/s	50 vol % N_2 + 50 vol % H_2O/0.072 m/s
f	LS + CS 2 (six chambers)	physical separation of char	N_2/0.144 m/s	N_2/0.8 m/s	50 vol % N_2 + 50 vol % H_2O/0.072 m/s

residence time of char also increases because of more chambers in the GCS; therefore, the conversion of char increases accordingly. With numerical studies on the design parameters, the optimal design can be determined to achieve a higher separation efficiency of CS and a long residence time of GCS. Detailed discussions about the newly designed device are shown in the following part.

3.2. Design of the CS. As mentioned in the Introduction, several kinds of CS developed by different researchers have the same principle and are based on the difference between the terminal velocity in the binary particle system involving the char and OC. The density of OC particles is higher than that of the char particles; therefore, the terminal velocity of char particles is lower, and it can be blown out more easily. Thus, the superficial fluidization velocity ranging between the terminal velocity of char and OC particles (0.30−1.46 m/s in this work) meets the requirement of separation. Moreover, the gasification process will further reduce the terminal velocity of char if these particles are recycled to the FR again; thus, it enhances the separation efficiency gradually until dynamic balance. Generally, only a small amount of char and ash fines flow out from the cyclone or slip to the AR, whereas with respect to GCS, its principle is quite different. The char slipping from the FR continues to be gasified in the GCS. The gasification products (instead of unburnt char) are recycled to the FR, and the combustible exhausts continue to react with OC in the FR, resulting in a higher carbon capture efficiency.

The structures of the CS and GCS adopted in this work are shown in Figure 3, where Figure 3a presents the first-generation LS + GCS (demonstrated in the 50 kW_{th} *i*G-CLC reactor[30]) and panels b and c of Figure 3 demonstrate the newly designed LS + CS/GCS. The basic targets for the design of the CS consist of minimizing the char slip, maximizing the separation efficiency, and minimizing the operational cost. The targets for the design of GCS are minimizing the char slip, prolonging the char residence time, and intensifying the gas−solid contact/mixture. In the new LS + CS/GCS, particles separated by the FR cyclone drop into the down comer, move downward in the moving bed, pass the supply chamber, then enter the chamber 1 from the inlet at the bottom, and move upward with the occurrence of physical separation. Next, particles cross the baffle, enter chamber 2, move downward, then enter chamber 3 and go up. After the particles pass through the baffle between chambers 3 and 4, they overflow to chamber 4 and flow to the recycle chamber at last. These chambers are connected in sequence as a S shape and separated by the baffle and clapboard. The baffle influences the height of the dense bed in the fluidized bed, then the bed inventory of the CS. The clapboard prevents the lateral movement of particles between chambers 1, 2 and chambers 3, 4 to make them flow along the scheduled route, which therefore lengthens the residence time of char in the CS/GCS. Basically, the CS/GCS can be divided into three zones along the direction of the height, containing the dense bed, freeboard, and transition zone. The dense bed is a bubbling/turbulent fluidized bed, and the height of it equals the height of the baffle. The freeboard is between the bottom bed and transition zone. The transition zone is pyramid-shaped and can elevate the local gas velocity and bring the gas/solid stream together to capture separated char easily.

Several key structure or operation parameters will affect the performance of the CS, such as the sectional area, bed inventory, baffle height, freeboard height, superficial velocity,

DOI: 10.1021/acs.energyfuels.9b02963
Energy Fuels 2019, 33, 12801−12813

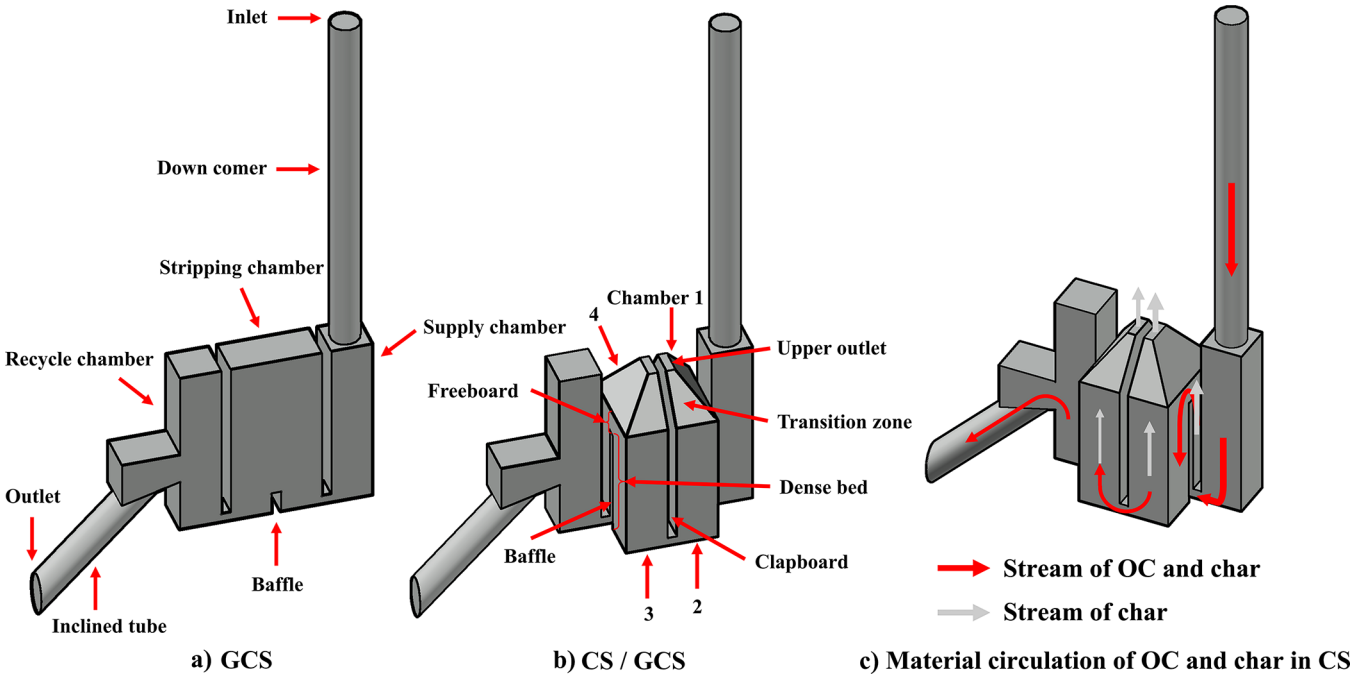

Figure 3. Structure of the CS and GCS.

Table 4. Parameters of the LS + CS/GCS for Simulations

parameter	value	parameter	value
sectional area (A_{CS}, m^2)	0.14	flow rate of char (F_{char}, kg/s)	0.2
superficial velocity of CS (V_{CS}, m/s) at H_{fre}, 0.1 m; H_{baf}, 0.3 m; and F_{OC}, 1.5 kg/s	0.4, 0.6, 0.8, 1, and 1.2	freeboard height (H_{fre}, m) at H_{baf}, 0.3 m; V_{CS}, 0.8 m/s; and F_{OC}, 1.5 kg/s	0.1, 0.2, 0.3, and 0.4
baffle height (H_{baf}, m) at H_{upp}, 0.1 m; V_{CS}, 0.8 m/s; and F_{OC}, 1.5 kg/s	0.2, 0.3, 0.4, and 0.5	flow rate of OC (F_{OC}, kg/s) at H_{fre}, 0.1 m; H_{baf}, 0.3 m; and V_{CS}, 0.8 m/s	0.5, 1, 1.5, 2, and 2.5

solid circulation rate, etc. They should be numerically designed and optimized to increase the separation efficiency. In this study, some of these parameters are optimized, as listed in Table 4. Simulations are performed to investigate the effects of the baffle height (H_{baf}), freeboard height (H_{fre}), superficial velocity (V_{CS}), and flow rate of OC (F_{OC}) on the separation efficiency of the CS. It should be noted that the possibility of capturing the char by the transition zone increases with the increase of the cross-section area, but the bed inventory and the operational cost also increase accordingly. Thus, there must be an optimal value, but in this work, the sectional area is fixed as 0.14 m^2. The CPFD simulation is only conducted with regard to the LS + CS/GCS, without FR and AR. Accordingly, the total flow rate of OC/char entering into the LS + CS/GCS is determined by the simulation results from strategy a, that is, 1.7 kg/s. The density of char particles is adopted as 1200 kg/m^3 after devolatilization and partial gasification. The initial bed height in each case is equal to the baffle height. The pressures at the inlet, outlet, upper outlet, and gas distributor are 101 557, 117 415, 119 000, and 101 325 Pa, respectively. The terminal velocity of char particles is 0.30 m/s, and that of OC particles is 1.46 m/s; therefore, the operational velocity in Table 4 varies from 0.4 to 1.2 m/s. To eliminate the effect of gasification, the fluidization agent in the simulations of single LS + CS is N_2 when studying the separation characteristics. The time step and resolutions of mesh and particle are in accordance with the simulation of the whole reactor. At last, considering the overall performance of the CS, the optimal design can be determined, and the GCS is based on the optimal structure as well.

4. RESULTS AND DISCUSSION

4.1. Separation Characteristics of the CS. The effects of the superficial velocity of the CS (V_{CS}), freeboard height (H_{fre}), baffle height (H_{baf}), and flow rate of OC at the inlet (F_{OC}) on the performance of the CS are shown in Figures 4−7, respectively, where the performance is evaluated by separation efficiency, η_{sep}, as shown in eq 1. η_{sep} stands for the ratio of char particles separated by the CS/specific chamber and recycled to the FR ($F_{char,CStoFR}$) to all char particles fed from the inlet at the top of the down comer ($F_{char,inlet}$).

$$\eta_{sep} = \frac{F_{char,CStoFR}}{F_{char,inlet}} \quad (1)$$

For the total separation efficiency of the CS under various conditions, V_{CS} and H_{fre} play crucial roles. With the increase of V_{CS}, total separation efficiency is improved to 95.7% at first (0.4−0.8 m/s) and then reaches a plateau. Considering the operational cost, the superficial velocity should be as low as possible with a relatively high performance; therefore, the optimal value is 0.8 m/s. In Figure 5, there is a negative correlation between H_{fre} and η_{sep} of the CS, because a lower freeboard height promotes char particles to be captured by the transition zone, i.e., improve the possibility to be separated. However, the freeboard zone cannot be canceled because if there is no freeboard between the dense bed and transition

DOI: 10.1021/acs.energyfuels.9b02963
Energy Fuels 2019, 33, 12801−12813

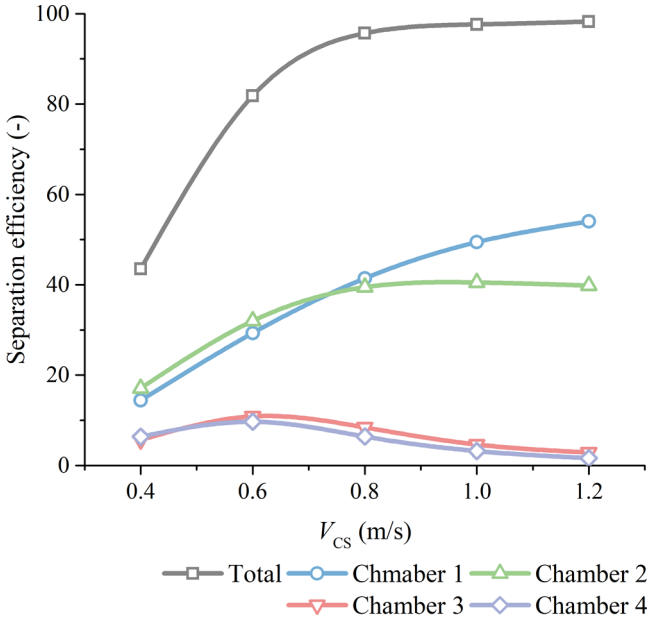

Figure 4. Separation efficiencies of the whole CS and each chamber under different V_{CS}.

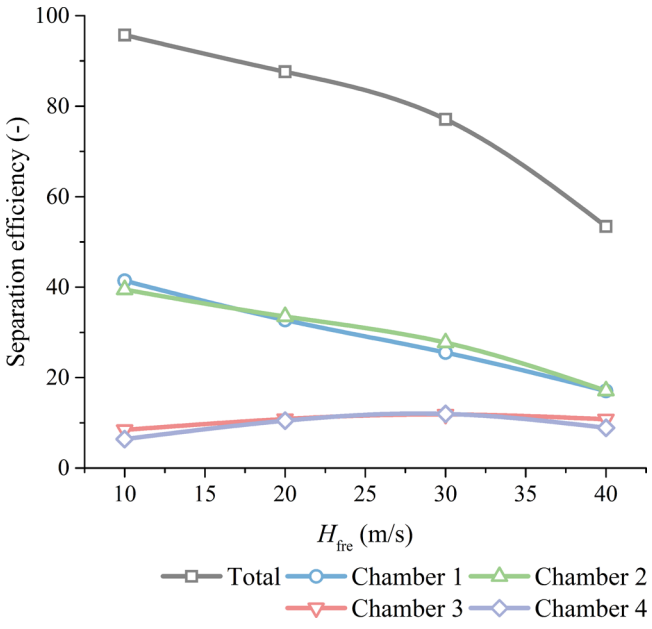

Figure 5. Separation efficiencies of the whole CS and each chamber under different H_{fre}.

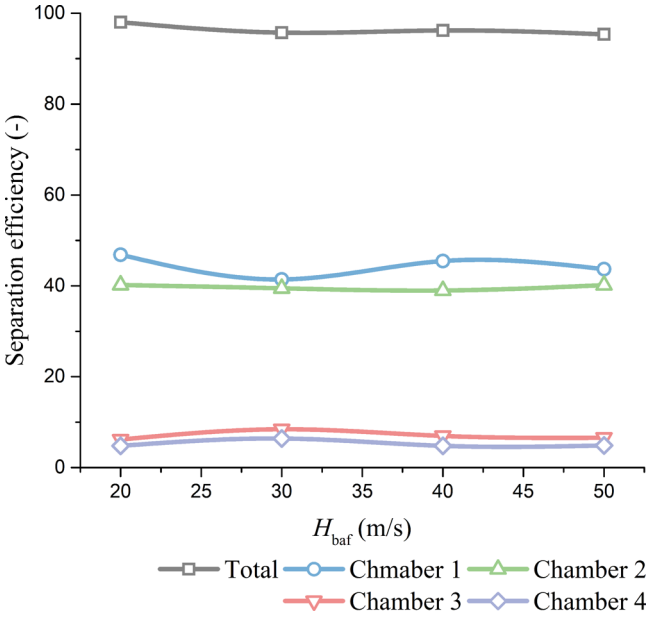

Figure 6. Separation efficiencies of the whole CS and each chamber under different H_{baf}.

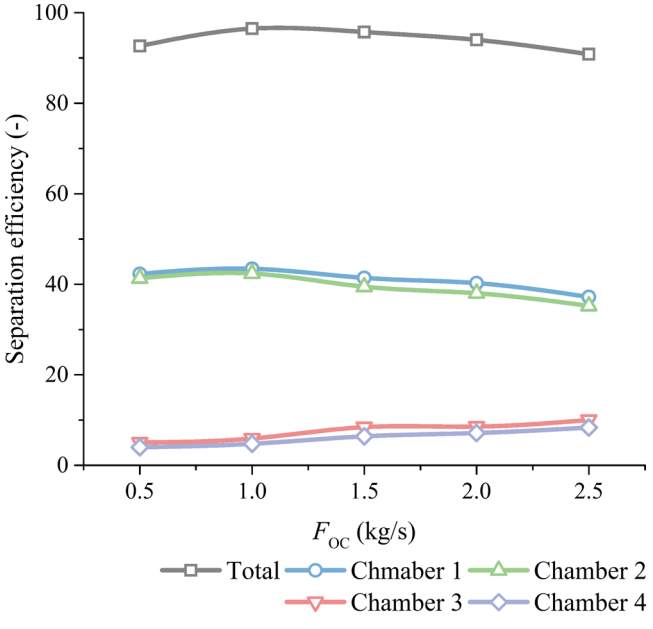

Figure 7. Separation efficiencies of the whole CS and each chamber under different F_{OC}.

zone, more OC will be blown out from the upper outlet of the CS and recycled to the FR. Eventually, the solid circulation rate to the AR cannot meet the requirement of basic operation. For the effects of the baffle height on separation characteristics, Figure 6 shows that η_{sep} does not change with the baffle height obviously. Therefore, in the CS mode, the baffle height is not a key parameter under a relatively high superficial velocity. However, in the GCS mode, the residence time of char particles in the GCS should be long enough for complete gasification, and it requires a longer reaction route, i.e., higher baffle height. Therefore, considering the influence of a higher bed height on operational cost, the optimal baffle height is 0.5 m. Finally, to evaluate the separation ability of CS under different solid circulation rates, the flow rate of OC is changed, as shown in Figure 7. η_{sep} slightly fluctuates with the change of F_{OC} and reaches the maximum of 96.5% at the total solid circulation rate of 1.2 kg/s. In the range of the total solid circulation rate from 0.7 to 2.7 kg/s, η_{sep} values are all higher than 90%, meaning that CS performs well on a relatively wide range of the solid circulation rate. In fact, the normal solid circulation rates of the 50 kW_{th} reactor are all distributed in this range. In conclusion, the optimal combination of design parameters to fulfill the requirements of the CS/GCS mode is "0.1 m H_{fre} + 0.5 m H_{baf} + 0.8 m/s V_{CS}".

Figures 4−7 also reveal the contributions of chambers 1−4 in the CS to the separation performance. First, in all chambers, chambers 1 and 2 have a similar performance and chambers 3 and 4 have a similar performance, because chambers 1 and 2

DOI: 10.1021/acs.energyfuels.9b02963
Energy Fuels 2019, 33, 12801−12813

and chambers 3 and 4 are connected at the top. Mixture stream flows along the fluidization gas in chambers 1 and 3 and flows against the fluidization gas in chambers 2 and 4. Thus, there are some little differences between the separation performance of chambers 1 and 2 and chambers 3 and 4. Second, chambers 1 and 2 always perform better than chambers 3 and 4 because these two chambers are in the upstream with more unseparated char. η_{sep} values of chambers 1 and 2 are distributed in 14.4−54.0%, and η_{sep} values of chambers 3 and 4 are distributed in 1.6−11.9%. Results also reveal that the tendency of η_{sep} of chambers 1 and 2 under different conditions always contrasts with that of chambers 3 and 4. Although the separation efficiencies of chambers 3 and 4 are lower than those of chambers 1 and 2, they are still of critical importance to the total performance, and this fact proves the superiority of four-chamber CS in comparison to the device with only two chambers.

4.2. Performance of Different Strategies to Promote Carbon Conversion. *4.2.1. Performance of Different Strategies to Prevent Char Slip.* Simulations are conducted to examine the performance of different strategies (shown in panels a−f of Figure 2) and explore how and why these strategies improve the carbon conversion. At the beginning, the char slip in the reactor is analyzed, and the results are shown in Figure 8. In the whole unit, there are several separated but

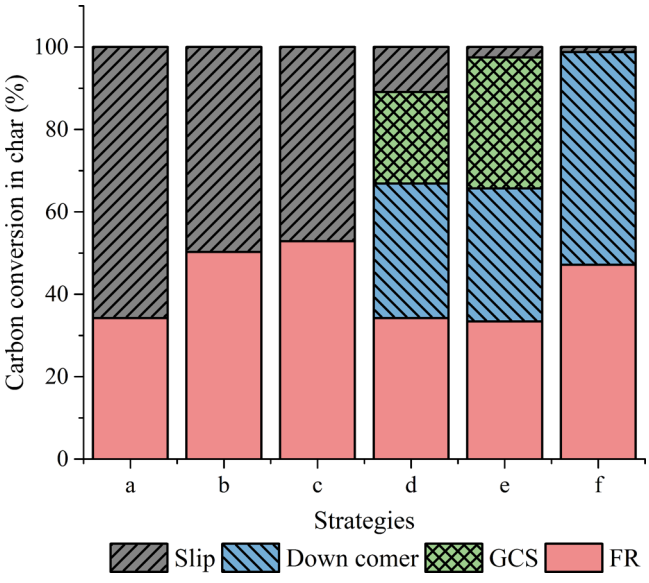

Figure 8. Carbon conversion in char employing different strategies.

sequentially connected parts for char gasification, that is, FR, down comer + supply chamber, and CS/GCS (in that order). Once the coal is fed to the FR, the char that is generated subsequently goes by these parts orderly, and this process will happen repeatedly if the CS is adopted. Thus, the specific percentage of char consumed in each part can be calculated one by one until it slips to the AR.

Figure 8 summarizes the char conversion experience and consumption share in various parts. First, it can be observed that, for a single FR without optimization (strategy a), the carbon conversion in char is merely around 34.2%, with the rest of 65.8% carbon slipping to the AR for air combustion, which is due to the relatively short residence time of char in the FR, and it is evidently harmful for CO_2 capture, whereas this phenomenon is relieved with the optimization of the FR in strategies b and c. The char slip is reduced to 49.8% with two oppositely collocated coal feeding points and 47.2% when doubling the FR height. The two strategies to extend the reaction route of char put positive effects on preventing char slip, but the conversions are still not satisfying. On the other side, the GCS can greatly promote the carbon conversion. Strategies d (LS + GCS 1) and e (LS + GCS 2) introduce a secondary place for char gasification beyond the FR, and these measures improve the carbon conversion obviously with the char slip ratio reducing to 10.9% in strategy d and 2.6% in strategy e.

Among different parts in the unit, the down comer + supply chamber is a main component for gasification in strategies d and e, which is similar to the char consumption share in FR because of the long residence time in the down comer and supply chamber. The residence time of char in the moving bed of the down comer + supply chamber can be approximately calculated through dividing the bed inventory by the solid circulation rate because of the uniform mixing of OC and char particles herein. As calculated, the bed inventory of it ranges from 60 to 70 kg and the solid circulation rate ranges from 0.6 to 2.2 kg/s; therefore, the residence time of char distributes in the range of 30−100 s, which is almost longer than that of 37 s in the FR. Moreover, the impacts of the GCS 1 and GCS 2 are also of crucial significance to char conversion, and the newly designed GCS 2 with more chambers performs better.

Strategy f in category 2 achieves the highest char conversion of 98.8% among all of the strategies, and the char slip in this case is quite small. Nearly all char particles circulate between the FR and CS. In the newly built internal loop, the conversion rate is lower than the accumulation rate at first, leading to the increase of the char circulation rate; thus, more char particles accumulate gradually until the dynamic balance between accumulation and consumption. On the basis of this, the concentration of char in the close loop, especially in the down comer and supply chamber, distinctly increases, in contrast with that without the CS, as shown in Figure 9. The higher char concentration leads to the higher conversion, and it further leads to the conspicuous improvement of char conversion in the down comer + supply chamber. In addition, because of the sequential circulation of char in "FR → down comer + supply chamber → CS → FR", the FR is always the first part where char particles pass by; therefore, the conversion in it is improved as well.

To investigate why the char conversion is promoted with a CS, the phenomenon of char accumulation is carefully analyzed, as seen in Figures 9 and 10. Figure 9a simulates the unit without a CS, and Figure 9b is equipped with a CS for physical separation. As discussed above, the employment of the CS promotes the char circulation in the newly built loop of char circulation, and it can be distinctly detected, as shown in Figure 10, which shows the evolution of the char circulation rate against time at the outlet of different components in the unit with a CS, including the FR, supply chamber, and CS. The char circulation rate at the outlet of each part increases gradually with little fluctuation. After 82 s, char outflow at the outlet of the FR (which includes the fresh char and recycled char) climbs over the value of fresh char fed from the coal feeding pipe (represented by the green dash in the graph). It means that the internal circulation of char is accelerated and more char accumulates in the loop. We can also find the evidence of the acceleration on char gasification in the down comer + supply chamber from the difference between the char

DOI: 10.1021/acs.energyfuels.9b02963
Energy Fuels 2019, 33, 12801−12813

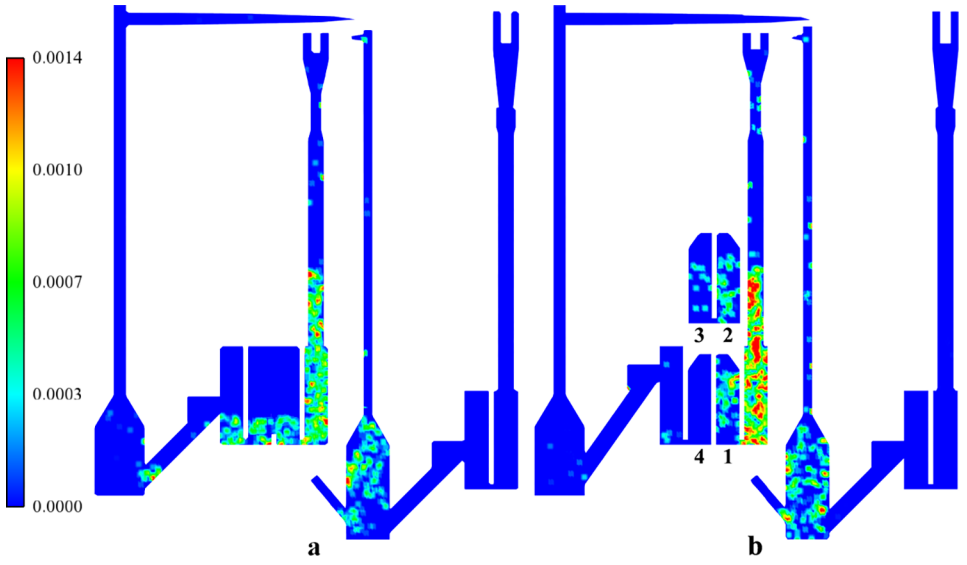

Figure 9. Carbon volume fraction in the unit (a) without a CS and (b) with a CS.

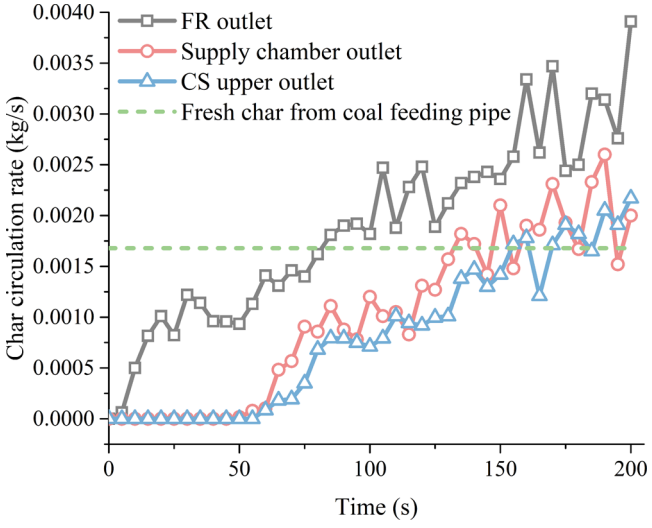

Figure 10. Evolution of the char circulation rate at the outlet of different components in the unit with the CS.

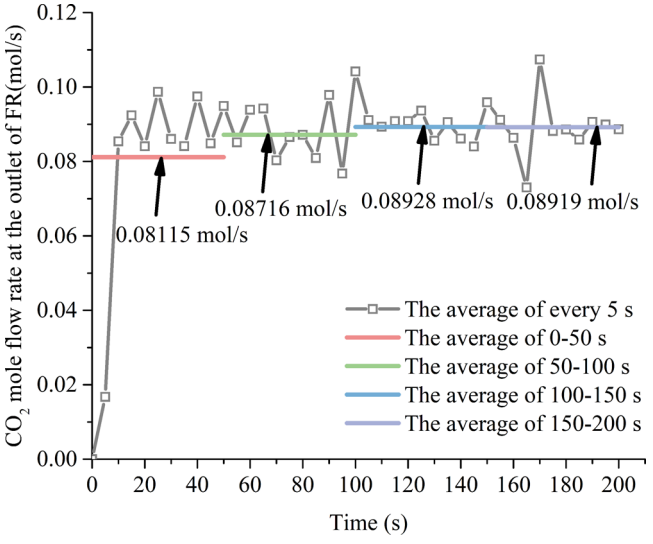

Figure 11. Evolution of the mole flow rate of CO_2 at the outlet of FR in the unit with the CS.

circulation rates monitored at the outlet of the FR and supply chamber. Moreover, it should be noted that the separation efficiency of the FR cyclone is relatively high, and few ash fines can flow out from the cyclone. Therefore, the curves of the char circulation rate (containing ash fines) keep rising in Figure 10, and it cannot be used as an index to determine whether and when the operation reaches a steady state. However, the exhaust concentration can be employed as the index. Figure 11 shows the evolution of the mole flow rate of CO_2 at the outlet of FR in the unit with the CS. It reveals that the reactions in the unit reach a steady state around 105 s; thus, we can conclude that the operation reaches a dynamic balance as well as the char circulation in the FR−CS loop. The additional increase of the char circulation rate after 105 s (there are time delays for the three curves; therefore, the values are higher for the CS and supply chamber) in Figure 10 is mainly from ash fines.

4.2.2. Performance of Different Strategies To Promote Fuel Gas Conversion. Apart from the promotion of char gasification, the conversion of fuel gases generated from the devolatilization and char gasification is also a crucial issue, which should be carefully studied. With the entrainment of fluidization gas, the volatiles always evolve to plume, which is hard to disperse to even half of the reactor, and they are the major parts of unburnt fuel gases. In contrast, the amount of unburnt fuel gases from char gasification is less because the rate of gasification is lower than the rates of heterogeneous reactions among OC and fuel gases, and the gasification products are mostly consumed after generated. Therefore, the optimal measures to promote fuel gas conversion should mainly pay attention to strengthen the mixture between fuel gases and OC and lengthen the route of heterogeneous reactions. Among different strategies, strategies b and c optimize the operation state of FR, putting a positive influence on the gas−solid mixing and reaction in it. Figure 12 shows the gas volume fractions of CO_2, CO, CH_4, and H_2 in FR exhausts. Indeed, in comparison to strategy a, the CO_2 concentration in strategies b and c increases, along with the decrease of combustible gases, and a higher FR in strategy c performs

DOI: 10.1021/acs.energyfuels.9b02963
Energy Fuels 2019, 33, 12801−12813

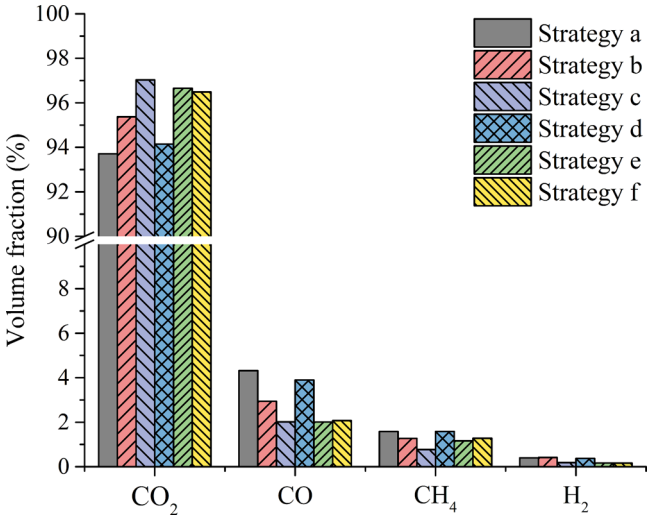

Figure 12. Gas volume fraction of CO_2, CO, CH_4, and H_2 in FR exhausts (dry basis and without N_2).

better than the multiple coal feeding point mode in strategy b. In contrast, strategies d–f focusing on the additional components beyond the FR also put positive effects on the fuel gas concentrations, and both the newly designed CS and GCS perform well. Figure 13 presents the carbon capture

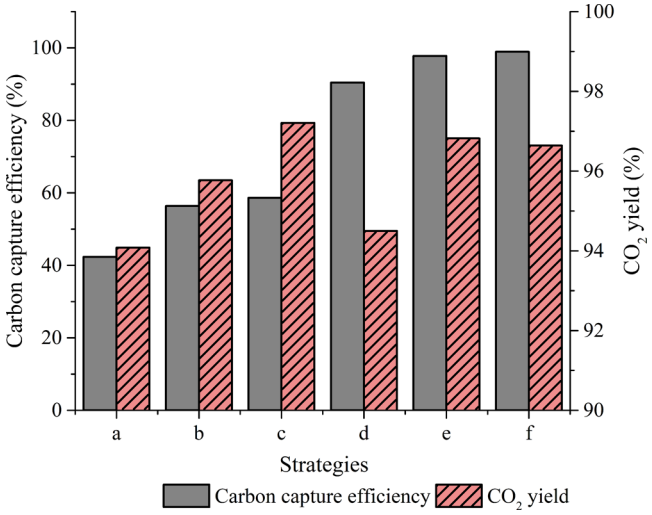

Figure 13. Carbon capture efficiency and CO_2 yield of the unit under different strategies.

efficiency (η_{CC}) and CO_2 yield (γ_{CO_2}) in various strategies. η_{CC} is calculated as eq 2, and $F_{i,AR/FR}$ is the mole flow rate of gas i at the outlet of the AR or FR. γ_{CO_2} is calculated as eq 3, and χ_i is the mole fraction of gas i at the outlet of the FR. It can be concluded that, to improve η_{CC}, one should focus on the optimizations beyond the FR, such as the introduction of CS or GCS. To improve γ_{CO_2}, one should focus on the optimizations of the FR as well as external devices.

$$\eta_{CC} = (F_{CO_2,FR} + F_{CO,FR} + F_{CH_4,FR}) / (F_{CO_2,AR} + F_{CO_2,FR} + F_{CO,FR} + F_{CH_4,FR}) \quad (2)$$

$$\gamma_{CO_2} = \chi_{CO_2} / (\chi_{CO} + \chi_{CH_4} + \chi_{CO_2}) \quad (3)$$

4.3. Operational Cost of Different Strategies. Table 5 shows the comparison of operational cost in different strategies, where the fan power (P_f) and steam generator power (P_s) are taken into consideration. It should be noted that the cost of preheating is not considered. The fan power represents the cost to overcome the pressure drop of the fluidized bed by the fan, which is calculated by the following equation:[41]

$$P_f = \frac{n}{(n-1)} \frac{p_1 \nu_a F_i}{\eta_{fan}} \left[\left[\frac{p_1 + \Delta p}{p_1} \right]^{(n-1)/n} - 1 \right] \quad (4)$$

where n is the isentropic coefficient, which is set as 1.4, p_1 is the inlet pressure of fan (here, it is assumed to be ambient), Δp is the pressure drop in each part, ν_a is the specific volume of fluidization gas at ambient temperature, F_i is the mass flow of air or N_2 in the fluidization agent, and η_{fan} is the efficiency of the fan, which is set as 0.9. The power of the steam generator represents the part of the operational cost to generate steam for char gasification, and it is calculated as eq 5

$$P_s = F_s \Delta H / \varepsilon_s \quad (5)$$

where F_s is the mass flow rate of steam, ΔH is the enthalpy change (kJ/kg) of water at ambient to steam at 1273 K, ε_s is the efficiency of the steam generator, which is set as 0.9. Because the steam does not flow through the fan, the cost of steam in fluidization gas just includes the part from the steam generator. Moreover, steam recycle from the outlet of the reactor is not taken into consideration in results of Table 5. Each component of the unit in different strategies, involving AR, AR LS, FR, FR LS, and CS/GCS, is included. On the basis of the total operational cost in strategies a–f, it can be found that the cost for steam generation accounts for the major part. Total costs in strategies a–c are approximate, and there are some little differences as a result of the change of bed inventory. However, in strategies d and e, the operational cost increases sharply with the employment of the GCS, especially in strategy e, which is 17.98 kW, and the operational cost of the GCS is even higher than that of the FR. However, in

Table 5. Comparison of the Operational Cost (Fan Power, P_f and Steam Generator Power, P_s)

	AR	AR LS	FR	FR LS	CS/GCS	
	P_f (W)	P_f (W)	P_f/P_s (W)	P_f/P_s (W)	P_f/P_s (W)	total (W)
a	323.2	60.9	115.6/6991.1	44.2/0	33.3/0	7568.3
b	316.7	60.9	115.8/6991.1	43.6/0	33.0/0	7561.1
c	296.2	92.0	174.0/7046	39.1/0	29.5/0	7676.8
d	323.2	60.9	115.6/6991.1	19.7/1620.9	15.0/1190.3	10336.7
e	354.6	70.8	128.6/6945.4	23.2/1995.1	123.0/8335.5	17976.2
f	361.5	69.0	126.4/6945.6	30.9/471.3	723.2/0	8727.9

DOI: 10.1021/acs.energyfuels.9b02963
Energy Fuels 2019, 33, 12801−12813

strategy f, despite the fact that the operational velocity of the CS is relatively high, the fan power demand is 0.72 kW and the total power demand is only 8.73 kW, which are lower than that of strategies d and e. All in all, considering the carbon capture efficiency and operational cost, strategy f with newly designed CS is also promising.

5. CONCLUSION

In this work, the CPFD method is adopted to investigate the carbon conversion, especially char conversion, in the full-scale 50 kW_{th} DCFB reactor for *i*G-CLC. Several strategies are put forward successively to promote the gas−solid reactions and improve the carbon conversion (consequently, attain higher carbon capture efficiency). In this article, strategies, such as the single FR, the multiple coal feeding mode, the higher FR, the original GCS (LS + GCS 1), the newly designed GCS (LS + GCS 2), and the newly designed CS (LS + CS 2), are marked as strategies a−f for simplification. Strategies a−e are based on extending the reaction route, and strategy f is based on recycling the residual char to the FR once again. Besides, strategies b and c intensify carbon conversion in the FR, whereas strategies d−f focus on the optimization beyond the FR. From the simulation results, a series of analyses about different strategies are conducted and compared, and the conclusions are shown as follows:

(1) A new four-chamber device coupled in a LS is designed with the help of numerical simulations. Several simulations of the integrated LS + CS (without the consideration of FR and AR) are conducted to regulate the crucial design parameters, such as freeboard height, baffle height, operational velocity, and flow rate of OC, and the optimal combination of "0.1 m H_{fre} + 0.5 m H_{baf} + 0.8 m/s V_{CS}" is eventually gained. The newly designed LS + CS (char is physically separated) can also be operated as LS + GCS (char is gasified herein, and actually, char is chemically separated) when the operational velocity decreases and the fluidization agent is changed to H_2O/CO_2.

(2) The performance of different strategies to prevent char slip is studied. The carbon conversion of char in each component of the reactor is carefully analyzed, involving the conversion in the FR, FR LS, GCS, and AR. For the comparison of char slip in different strategies, 65.8% carbon slips to the AR for combustion in the single FR (strategy a), but the char slip is relieved under strategies b−f, being reduced to 49.8, 47.2, 10.9, 2.6, and 1.2%, respectively. Among each part, the supply chamber + down comer and/or GCS play important roles in the process of char gasification, and the supply chamber + down comer is especially important in strategy f because an extra char circulation is built in the system and the char concentration accordingly increases. Moreover, to improve the carbon capture efficiency, the optimizations beyond the FR, such as the introduction of CS/GCS, are necessary.

(3) Combustible gas conversion in the unit under various strategies is also investigated, and the exhaust gas concentrations at the outlet of the FR cyclone are compared. It can be found that the gas concentrations are obviously various as a result of the change in the FR, such as strategies b and c, and the higher FR performs better than other strategies. The external devices beyond the FR also put considerable influence on the exhaust compositions. To improve the CO_2 yield, one should focus on the optimizations of the FR as well as external devices (e.g., the introduction of CS/GCS to enhance the combustible gas concentrations and then their conversion in the FR).

(4) At last, the operational costs of the fan and steam generator for the fluidization gases in every component are calculated and compared. Considering the carbon conversion and operational cost, the optimal strategy can be determined. Strategy f has the lowest char slip, considerable combustible gas conversion, and relatively lower operational cost. The newly designed CS finally makes the balance between the performance and operational cost.

■ ASSOCIATED CONTENT

Supporting Information

The Supporting Information is available free of charge at https://pubs.acs.org/doi/10.1021/acs.energyfuels.9b02963.

CPFD model and model/simulation validation (PDF)

■ AUTHOR INFORMATION

Corresponding Author

*E-mail: hzhao@mail.hust.edu.cn

ORCID

Haibo Zhao: 0000-0002-2693-4499

Notes

The authors declare no competing financial interest.

■ ACKNOWLEDGMENTS

The authors acknowledge the support from the "National Key R&D Program of China (2018YFB0605404)".

■ REFERENCES

(1) Kolbitsch, P.; Pröll, T.; Bolhar-Nordenkampf, J.; Hofbauer, H. Design of a chemical looping combustor using a dual circulating fluidized bed reactor system. *Chem. Eng. Technol.* **2009**, *32* (3), 398−403.

(2) Markström, P.; Lyngfelt, A. Designing and operating a cold-flow model of a 100kW chemical-looping combustor. *Powder Technol.* **2012**, *222*, 182−192.

(3) Linderholm, C.; Lyngfelt, A.; Cuadrat, A.; Jerndal, E. Chemical-looping combustion of solid fuels−Operation in a 10kW unit with two fuels, above-bed and in-bed fuel feed and two oxygen carriers, manganese ore and ilmenite. *Fuel* **2012**, *102*, 808−822.

(4) Ma, J.; Zhao, H.; Tian, X.; Wei, Y.; Rajendran, S.; Zhang, Y.; Bhattacharya, S.; Zheng, C. Chemical looping combustion of coal in a 5 kW_{th} interconnected fluidized bed reactor using hematite as oxygen carrier. *Appl. Energy* **2015**, *157*, 304−313.

(5) Sun, H.; Cheng, M.; Li, Z.; Cai, N. Riser-based carbon stripper for coal-fueled chemical looping combustion. *Ind. Eng. Chem. Res.* **2016**, *55* (8), 2381−2390.

(6) Lyngfelt, A.; Leckner, B. A 1000 MW_{th} boiler for chemical-looping combustion of solid fuels−Discussion of design and costs. *Appl. Energy* **2015**, *157*, 475−487.

(7) Gayán, P.; Abad, A.; de Diego, L. F.; García-Labiano, F.; Adánez, J. Assessment of technological solutions for improving chemical looping combustion of solid fuels with CO_2 capture. *Chem. Eng. J.* **2013**, *233*, 56−69.

(8) Sozinho, T.; Pelletant, W.; Stainton, H.; Guillou, F.; Gauthier, T. Main results of the 10 kW_{th} pilot plant operation. *Proceedings of the 2nd International Conference on Chemical Looping*; Darmstadt, Germany, Sept 26−28, 2012.

(9) Shen, L.; Wu, J.; Xiao, J. Experiments on chemical looping combustion of coal with a NiO based oxygen carrier. *Combust. Flame* **2009**, *156* (3), 721−728.

(10) García-Labiano, F.; de Diego, L. F.; Gayán, P.; Abad, A.; Adánez, A. Fuel reactor modelling in chemical-looping combustion of

DOI: 10.1021/acs.energyfuels.9b02963
Energy Fuels 2019, 33, 12801−12813

coal: 2—Simulation and optimization. *Chem. Eng. Sci.* **2013**, *87*, 173−182.
(11) Cuadrat, A.; Abad, A.; Gayán, P.; De Diego, L. F.; García-Labiano, F.; Adánez, J. Theoretical approach on the CLC performance with solid fuels: Optimizing the solids inventory. *Fuel* **2012**, *97*, 536−551.
(12) Ströhle, J.; Orth, M.; Epple, B. Design and operation of a 1 MW_{th} chemical looping plant. *Appl. Energy* **2014**, *113*, 1490−1495.
(13) Kim, H. R.; Wang, D.; Zeng, L.; Bayham, S.; Tong, A.; Chung, E.; Kathe, M. V.; Luo, S.; McGiveron, O.; Wang, A.; Sun, Z.; Chen, D.; Fan, L.-S. Coal direct chemical looping combustion process: Design and operation of a 25-kW_{th} sub-pilot unit. *Fuel* **2013**, *108*, 370−384.
(14) Thon, A.; Kramp, M.; Hartge, E. U.; Heinrich, S.; Werther, J. Operational experience with a system of coupled fluidized beds for chemical looping combustion of solid fuels using ilmenite as oxygen carrier. *Appl. Energy* **2014**, *118*, 309−317.
(15) Sun, H.; Xu, L.; Li, Z.; Cai, N. Investigation of a coupled fuel reactor for coal-fueled chemical looping combustion. *Ind. Eng. Chem. Res.* **2014**, *53* (39), 15157−15166.
(16) Abad, A.; Pérez-Vega, R.; Mendiara, T.; Gayán, P.; Adánez, J. Improving the performance of the chemical looping combustion process with coal in a 50 kW_{th} unit. *Proceedings of the 5th International Conference on Chemical Looping*; Park City, UT, Sept 24−27, 2018.
(17) Guío-Pérez, D. C.; Hofbauer, H.; Pröll, T. Effect of ring-type internals on solids distribution in a dual circulating fluidized bed system−cold flow model study. *AIChE J.* **2013**, *59* (10), 3612−3623.
(18) Schmid, J. C.; Pröll, T.; Kitzler, H.; Pfeifer, C.; Hofbauer, H. Cold flow model investigations of the countercurrent flow of a dual circulating fluidized bed gasifier. *Biomass Convers. Biorefin.* **2012**, *2* (3), 229−244.
(19) Chen, X.; Ma, J.; Tian, X.; Wan, J.; Zhao, H. CPFD simulation and optimization of a 50 kW_{th} dual circulating fluidized bed reactor for chemical looping combustion of coal. *Int. J. Greenhouse Gas Control* **2019**, *90*, 102800.
(20) Zhao, H.; Tian, X.; Ma, J.; Su, M.; Wang, B.; Mei, D. Development of tailor-made oxygen carriers and reactors for chemical looping processes at Huazhong University of Science and Technology. *Int. J. Greenhouse Gas Control* **2019**, 102898.
(21) Berguerand, N.; Lyngfelt, A. Design and operation of a 10 kW_{th} chemical-looping combustor for solid fuels−Testing with South African coal. *Fuel* **2008**, *87* (12), 2713−2726.
(22) Markström, P.; Lyngfelt, A. Designing and operating a cold-flow model of a 100kW chemical−looping combustor. *Powder Technol.* **2012**, *222*, 182−192.
(23) Mendiara, T.; Gayán, P.; Abad, A.; De Diego, L. F.; García-Labiano, F.; Adánez, J. Performance of a bauxite waste as oxygen-carrier for chemical-looping combustion using coal as fuel. *Fuel Process. Technol.* **2013**, *109*, 57−69.
(24) Abad, A.; Adánez, J.; de Diego, L. F.; Gayán, P.; García-Labiano, F.; Lyngfelt, A. Fuel reactor model validation: Assessment of the key parameters affecting the chemical-looping combustion of coal. *Int. J. Greenhouse Gas Control* **2013**, *19*, 541−551.
(25) Abad, A.; Pérez-Vega, R.; De Diego, L. F.; García-Labiano, F.; Gayán, P.; Adánez, J. Design and operation of a 50 kW_{th} Chemical Looping Combustion (CLC) unit for solid fuels. *Appl. Energy* **2015**, *157*, 295−303.
(26) Abad, A.; Adánez, J.; Gayán, P.; De Diego, L. F.; García-Labiano, F.; Sprachmann, G. Conceptual design of a 100 MW_{th} CLC unit for solid fuel combustion. *Appl. Energy* **2015**, *157*, 462−474.
(27) Sun, H.; Cheng, M.; Chen, D.; Xu, L.; Li, Z.; Cai, N. Experimental study of a carbon stripper in solid fuel chemical looping combustion. *Ind. Eng. Chem. Res.* **2015**, *54* (35), 8743−8753.
(28) Cheng, M.; Li, Y.; Li, Z.; Cai, N. An integrated fuel reactor coupled with an annular carbon stripper for coal-fired chemical looping combustion. *Powder Technol.* **2017**, *320*, 519−529.
(29) Abdulally, I.; Beal, C.; Andrus, H.; Epple, B.; Lyngfelt, A.; Lani, B. Alstom's chemical looping prototypes, program update. *Proceedings of the 37th International Technical Conference on Clean Coal & Fuel Systems*; Clearwater, FL, June 3−7, 2012.
(30) Ma, J.; Tian, X.; Wang, C.; Chen, X.; Zhao, H. Performance of a 50 kW_{th} coal-fuelled chemical looping combustor. *Int. J. Greenhouse Gas Control* **2018**, *75*, 98−106.
(31) Andrews, M. J.; O'Rourke, P. J. The multiphase particle-in-cell (MP-PIC) method for dense particulate flows. *Int. J. Multiphase Flow* **1996**, *22*, 379−402.
(32) Snider, D. M. An incompressible three-dimensional multiphase particle-in-cell model for dense particle flows. *J. Comput. Phys.* **2001**, *170*, 523−549.
(33) Mahalatkar, K.; Kuhlman, J.; Huckaby, E. D.; O'Brien, T. Computational fluid dynamic simulations of chemical looping fuel reactors utilizing gaseous fuels. *Chem. Eng. Sci.* **2011**, *66*, 469−479.
(34) Su, M.; Zhao, H.; Ma, J. Computational fluid dynamics simulation for chemical looping combustion of coal in a dual circulation fluidized bed. *Energy Convers. Manage.* **2015**, *105*, 1−12.
(35) Parker, J. M. CFD model for the simulation of chemical looping combustion. *Powder Technol.* **2014**, *265*, 47−53.
(36) Deng, Z.; Xiao, R.; Jin, B.; Song, Q. Numerical simulation of chemical looping combustion process with CaSO4 oxygen carrier. *Int. J. Greenhouse Gas Control* **2009**, *3*, 368−375.
(37) Jung, J.; Gamwo, I. K. Multiphase CFD-based models for chemical looping combustion process: Fuel reactor modeling. *Powder Technol.* **2008**, *183*, 401−409.
(38) Wang, S.; Lu, H.; Zhao, F.; Liu, G. CFD studies of dual circulating fluidized bed reactors for chemical looping combustion processes. *Chem. Eng. J.* **2014**, *236*, 121−130.
(39) Su, M.; Zhao, H. Modifying the inter-phase drag via solid volume fraction gradient for CFD simulation of fast fluidized beds. *AIChE J.* **2017**, *63*, 2588−2598.
(40) Shao, Y.; Zhang, Y.; Wang, X.; Wang, X.; Jin, B.; Liu, H. Three dimensional full loop modeling and optimization of an in situ gasification chemical looping combustion system. *Energy Fuels* **2017**, *31*, 13859−13870.
(41) Lyngfelt, A.; Leckner, B.; Mattisson, T. A fluidized-bed combustion process with inherent CO_2 separation; Application of chemical-looping combustion. *Chem. Eng. Sci.* **2001**, *56* (10), 3101−3113.

DOI: 10.1021/acs.energyfuels.9b02963
Energy Fuels 2019, 33, 12801−12813